# Mitochondrial Mutations Contribute to HIF1α Accumulation via Increased Reactive Oxygen Species and Up-regulated Pyruvate Dehydrogenase Kinase 2 in Head and Neck Squamous Cell Carcinoma

Wenyue Sun,[1] Shaoyu Zhou,[1] Steven S. Chang,[1] Thomas McFate,[2] Ajay Verma,[2] and Joseph A. Califano[1]

**Abstract**

**Purpose:** Mitochondrial mutations have been identified in head and neck squamous cell carcinoma (HNSCC), but the pathways by which phenotypic effects of these mutations are exerted remain unclear. Previously, we found that mitochondrial ND2 mutations in primary HNSCC increased reactive oxygen species (ROS) and conferred an aerobic, glycolytic phenotype with HIF1α accumulation and increased cell growth. The purpose of the present study was to examine the pathways relating these alterations.

**Experimental Design:** Mitochondrial mutant and wild-type *ND2* constructs were transfected into oral keratinocyte immortal cell line OKF6 and head and neck cancer cell line JHU-O19 and established transfectants. The protein levels of HIF1α, pyruvate dehydrogenase (PDH), phosphorylated PDH, and pyruvate dehydrogenase kinase 2 (PDK2), together with ROS generation, were compared between the mutant and the wild type. Meanwhile, the effects of small molecule inhibitors targeting PDK2 and mitochondria-targeted catalase were evaluated on the ND2 mutant transfectants.

**Results:** We determined that ND2 mutant down-regulated PDH expression via up-regulated PDK2, with an increase in phosphorylated PDH. Inhibition of PDK2 with dichloroacetate decreased HIF1α accumulation and reduced cell growth. Extracellular treatment with hydrogen peroxide, a ROS mimic, increased PDK2 expression and HIF1α expression, and introduction of mitochondria-targeted catalase decreased mitochondrial mutation-mediated PDK2 and HIF1α expression and suppressed cell growth.

**Conclusions:** Our findings suggest that mitochondrial ND2 mutation contributes to HIF1α accumulation via increased ROS production, up-regulation of PDK2, attenuating PDH activity, thereby increasing pyruvate, resulting in HIF1α stabilization. This may provide insight into a potential mechanism, by which mitochondrial mutations contribute to HNSCC development.

Human mitochondrial DNA (mtDNA) is a circular double-stranded DNA ~16.6 kb in size. It encodes 13 polypeptides, which includes seven subunits (ND1-ND6, ND4L) of respiratory chain complex I, one subunit (CYTB) of complex III, three subunits (COI-COIII) of complex IV, and two subunits (ATP6 and ATP8) of complex V, 22 tRNAs, and 2 rRNAs (1). Human mtDNA is more susceptible to damage than nuclear DNA, as the mtDNA molecule is not protected by histones, is exposed to reactive oxygen species (ROS) generated during oxidative phosphorylation, and is replicated by DNA polymerase γ, which copies with low fidelity due to the absence of a proofreading function (2).

Somatic mtDNA mutations have been increasingly observed in primary human cancers (3). In head and neck squamous cell carcinoma (HNSCC), studies have shown a frequency of mitochondrial mutations ranging from 21% to 51%. Of note, our recent study found a nonrandom distribution of mitochondrial mutation throughout the mitochondrial enzyme complex components (4), and the majority of mitochondrial mutations occur during or after the transition of preneoplastic epithelium to cancer in HNSCC, indicating that these are a late event in HNSCC carcinogenesis (5).

Mitochondrial defects have long been suspected to play an important role in the development of cancer. Over 70 years ago, Otto Warburg described that cancer cells had impaired mitochondrial respiratory function compared with normal cells

**Authors' Affiliations:** [1]Department of Otolaryngology-Head and Neck Surgery, Johns Hopkins Medical Institutions, Baltimore, Maryland and [2]Department of Neurology, Uniformed Services University of the Health Sciences, Bethesda, Maryland

Received 4/9/08; revised 9/22/08; accepted 9/22/08.

**Grant support:** Specialized Program of Research Excellence grant P50 CA96784. J.A. Califano is a Damon Runyon-Lilly Clinical Investigator supported by the Damon Runyon Cancer Research Foundation (CI-#9), a Clinical Innovator Award from Flight Attendant Medical Research Institute, and National Institute of Dental and Craniofacial Research grant 1R01DE015939-01.

The costs of publication of this article were defrayed in part by the payment of page charges. This article must therefore be hereby marked *advertisement* in accordance with 18 U.S.C. Section 1734 solely to indicate this fact.

**Note:** Supplementary data for this article are available at Clinical Cancer Research Online (http://clincancerres.aacrjournals.org/).

**Requests for reprints:** Joseph A. Califano, Department of Otolaryngology-Head and Neck Surgery, Johns Hopkins Medical Institutions, Baltimore, MD 21287. Phone: 410-955-6420; Fax: 410-955-8510; E-mail: jcalifa@jhmi.edu.



doi:10.1158/1078-0432.CCR-08-0930

## Translational Relevance

Mitochondrial DNA (mtDNA) mutations occur with high frequency in a variety of human tumors, but the functional consequences of such mutations are unknown. We reported here the novel mechanism of mitochondrial mutation-mediated cancer carcinogenesis. The mtDNA mutations contribute to malignant phenotype via increased ROS, up-regulation of PDK2, attenuating PDH activity, elevating pyruvate production, and thereby HIF1α stabilization. Interestingly, ROS scavenger, PDK2 inhibitor dichloroacetate, and HIF1α small molecule inhibitor inhibit the malignant phenotypes induced by mitochondrial mutations. Our results not only provide mechanistic insight into the functional role of mtDNA mutations in human cancers but also open an important avenue for pharmacologic perturbation of this important pathway, which benefits the patients harboring mtDNA mutations.

(6). He noted that cancer cells typically depend more on increased rates of glycolysis even in the presence of available oxygen, a phenomenon known as aerobic glycolysis or the Warburg effect. The Warburg effect is now considered a common property of cancer metabolism (7). Recently, studies from Lu and colleagues suggested that glycolytic products, like pyruvate, lead directly to HIF1α activation; this further boosts metabolism, as well as stimulates angiogenesis and invasiveness, and in turn confers a growth advantage to cells (8).

Previously, we reported that nuclear-transcribed, mitochondrial-targeted, mitochondrial ND2 protein mutants could induce increased ROS generation, elevated glycolytic metabolism, and enhanced HIF1α accumulation (4). The purpose of the present study was to discover the functional network mediated by mitochondrial mutation elucidating the above phenomenon. Here, we report that this mitochondrial mutation contributes to HIF1α accumulation via increased ROS production, up-regulation of pyruvate dehydrogenase kinase 2 (PDK2), decreasing pyruvate dehydrogenase (PDH) activity, and elevating pyruvate concentration, resulting in HIF1α stabilization.

## Materials and Methods

***Cell culture.*** HeLa cells were grown in DMEM supplemented with 10% fetal bovine serum. Human HNSCC cancer cell line JHU-O19, established at the Johns Hopkins University Department of Otolaryngology-Head and Neck Surgery, were grown in RPMI 1640 supplemented with 10% fetal bovine serum. Human oral keratinocyte immortal cell line OKF6, purchased from the Rheinwald Laboratory (Brigham and Women's Hospital), were grown in defined keratinocyte serum-free medium with defined growth supplement and a final $Ca^{2+}$ concentration of 0.4 mmol/L. All of the cells were supplemented with 1% (v/v) penicillin/streptomycin. The components of Krebs-Henseleit buffer were 5.5 mmol/L glucose, 1.3 mmol/L $CaCl_2$, 1.3 mmol/L $MgCl_2$, 124 mmol/L NaCl, 3.5 mmol/L KCl, 1.25 mmol/L $K_2HPO_4$, and 26.3 mmol/L $NaHCO_3$ (pH 7.5), after bubbling with 5% $CO_2$ in air. Where indicated, glucose was replaced by the indicated concentrations of agents.

***Antibodies and reagents.*** Mouse monoclonal anti-HIF1α antibodies were purchased from BD Biosciences. Rabbit polyclonal anti-PDK2 antibodies were purchased from Abgent. Rabbit polyclonal anticatalase antibodies were obtained from Calbiochem. Rabbit polyclonal anti–phosphorylated PDH antibodies were generated from Dr. Verma's laboratory. Mouse monoclonal anti-PDH E1α subunit antibody and 2′,7′-dichlorofluorescein diacetate (DCFH-DA) were from Invitrogen. Dichloroacetate and catalase from human erythrocytes were purchased from Sigma. The HIF1α small molecule inhibitor NSC134754 was obtained from National Cancer Institute through their Developmental Therapeutic Program. Mitochondria-targeted catalase (mito-cat) construct was a gift from Dr. Lenzen (Hannover Medical School).

***Plasmid construction.*** We converted the *ND2* gene into nuclear code directly by using long-range gene synthesis, as previously described (4). With this long-range gene synthesis technique, we synthesized *ND2* wild type and one mutant, mt1 (*ND2*-G4776A; amino acid change A-T). The synthesized wild type and mutants then were subcloned into *Sal*I and *Not*I sites of plasmid pCMV/myc/mito (Invitrogen). Plasmids were resequenced with conventional sequencing to confirm results.

***Transfection of ND2 constructs.*** HeLa cells, O19 cells, and OKF6 immortal keratinocytes were transfected with empty vector, wild type, or mutant construct at 40% to 60% confluence by using FuGENE 6 (Roche), according to product protocols.

***Pyruvate measurement.*** To measure pyruvate, 50 μL of medium were taken from cells grown in 2 mL of medium in six-well cell culture plates and frozen until the time of measurement. Before measurement, samples were centrifuged to remove any microbubbles. Pyruvate content was measured by the enzymatic method using a pyruvate kit (CMA microdialysis). Metabolite measurements were done with the CMA 600 Analyzer.

***ROS measurement.*** Intracellular ROS generation was assessed using DCFH-DA with the method described previously (9). Briefly, cells were plated on Petri dishes and incubated with DCFH-DA (10 μmol/L) under various conditions. The cells were lysed and centrifuged to remove debris, and the fluorescence in the supernatant was measured using a spectrofluorometer (excitation, 500 nm; emission, 530 nm). Data were normalized to values obtained from untreated controls.

***Western blotting.*** Cells were lysed in radioimmunoprecipitation assay buffer supplemented with proteinase inhibitor. Whole protein extracts (~30 μg) were resolved on a 4% to 10% NuPAGE gel (Invitrogen), transferred to a polyvinylidene fluoride membrane (Amersham Biosciences), probed overnight at 4°C with the antibody against PDK2, PDH, p-PDH, HIF1α, catalase, and actin, and then revealed using the enhanced chemiluminescence system (Roche). Densitometry was done using Image J software (NIH).

***Sulforhodamine-B assay.*** Growth inhibition was evaluated using the sulforhodamine B assay, as previously described (10). Briefly, cells were plated into clear, flat-bottomed 96-well plates and were left to attach overnight. They were treated with the indicated agents and incubated for 48 to 72 h. At the end of the incubation period, the cells were fixed and stained with sulforhodamine B (Sigma). The absorbance value was read at a wavelength of 540 to 570 nm. The cell survival was presented as the percentage of control, as calculated by using the equation: $A_t/A_c \times 100$, wherein $A_t$ and $A_c$ represent the absorbance in treated and control cultures, respectively.

***Tumor xenografts.*** For tumor growth, $2 \times 10^6$ cells in 100 μL PBS were injected s.c. at the left flank of 4-wk-old to 6-wk-old female athymic nude mice (CD-1-nuBR, Charles River). All experiments were done in accordance with the Johns Hopkins University Animal Care and Use Committee guideline. Each group consisted of five mice. Tumor growth was monitored weekly, and mice showing signs of morbidity were immediately sacrificed according to the university guidelines. Tumor volume was calculated with slide calipers using the following formula: $V$ = width × width × length × 0.5, wherein $V$ is volume ($mm^3$).

*Statistical analysis.* Differences between experimental variables were estimated using Student's *t* test. A probability level of 0.05 was chosen for statistical significance. The columns in the histograms represent the mean ± SD of at least triplicate values from independent experiments.

## Results

***Mitochondrial ND2 mutant promotes head and neck cancer cell growth through HIF1α accumulation.*** Recently, we reported that expression of nuclear-transcribed, mitochondrial-targeted ND2 mutant resulted in anchorage-independent growth and HIF1α accumulation. To further examine this phenomenon, one mitochondrial *ND2* mutant construct (mt1; ND2-G4776A, amino acid change A→T, which were originally found in human primary HNSCC cancers) was established. We transfected this mutant into HeLa cells, immortal keratinocyte OKF6 cells, and O19 head and neck cell line (*ND2* wild-type background), respectively. Western blot analysis showed that HIF1α was overexpressed in all three cells transfected with mitochondrial *ND2* mutant versus their corresponding wild-type *ND2* construct (Fig. 1A), with 3.0 ± 0.9-fold (mean ± SD, $n = 3$, $P = 0.012$), 4.0 ± 1.7-fold (mean ± SD, $n = 3$, $P = 0.034$), and 2.5 ± 0.4-fold (mean ± SD, $n = 3$, $P = 0.010$), respectively. Consistently, the ND2 mutant exhibited increased proliferation rates compared with the wild type in HeLa cells and O19 cells (Fig. 1B and C; $P < 0.01$). In our study, we also found that HeLa cells stably transfected with *ND2* mutant significantly increased the tumor growth in nude mice compared with the wild type (Supplementary Fig. S1; $P < 0.01$). Furthermore, we found that treatment with 0.5 μmol/L HIF1α small molecule inhibitor NSC134754, the cell growth advantage conferred by the mitochondrial ND2 mutant in HeLa cells and O19 cells, was completely eliminated at 48 hours (Fig. 1B and C; ref. 11). Taken together, these suggest that HIF1α accumulation is a major mechanism of mitochondrial mutation-induced growth for ND2 mutants.

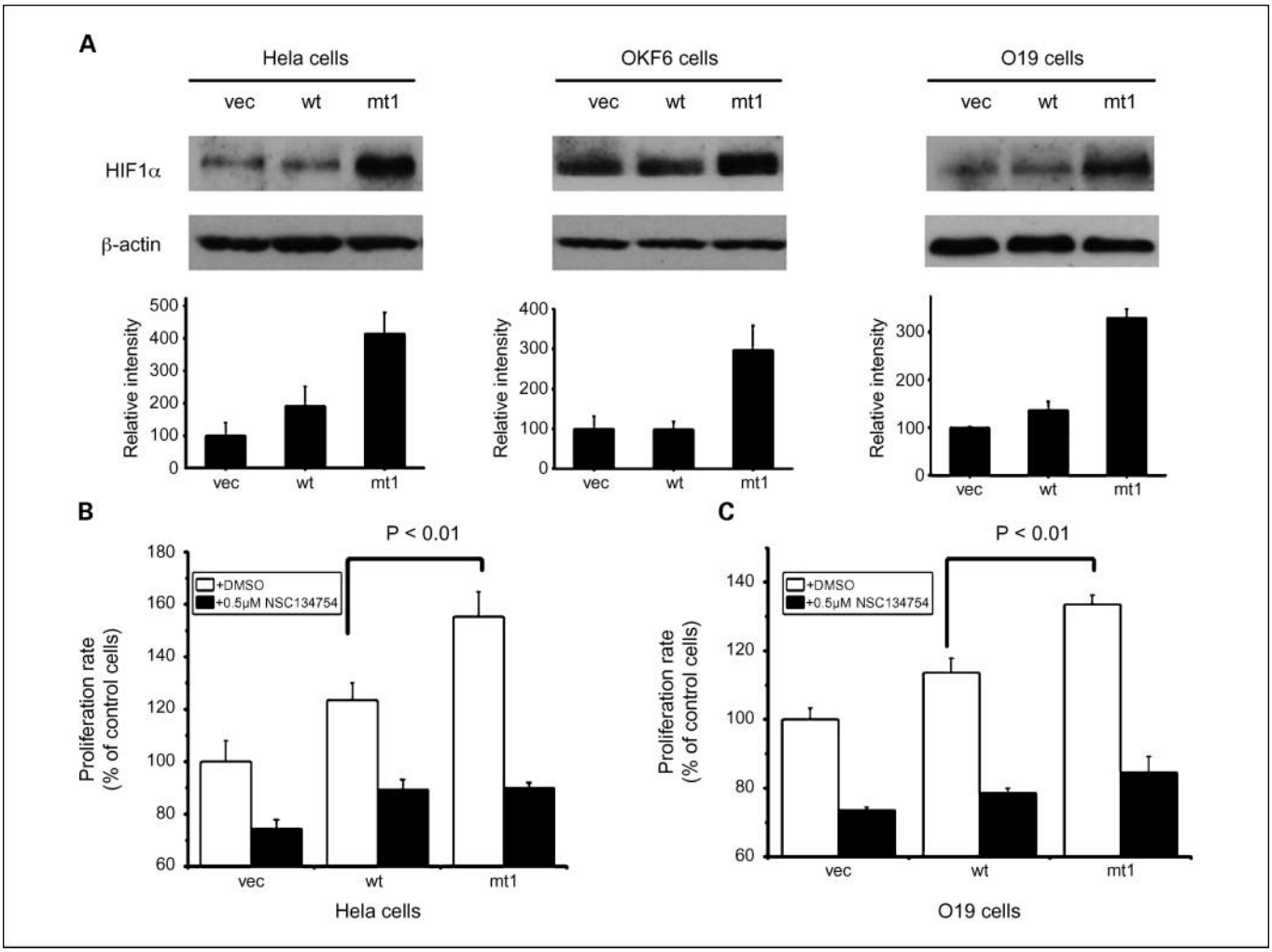


**Fig. 1.** Mitochondrial ND2 mutant promoted head and neck cancer cell growth through HIF1α accumulation. *A,* the protein levels of HIF1α were determined 4 h after switching from culture medium to Krebs-Henseleit buffer in HeLa, OKF6, and O19 cells. Immunoblots were quantified via densitometry and Image J software. HIF1α was overexpressed by 3.0 ± 0.9-fold, 4.0 ± 1.7-fold, and 2.5 ± 0.4-fold in the three cells transfected with mitochondrial ND2 mutant versus their corresponding wild type ($n = 3$, $P < 0.05$). Representative images from three independent experiments. *B,* the growth of HeLa cells stably transfected with ND2 mutant was inhibited after treatment with NSC134754, a HIF1α small inhibitor. Cell growth was estimated by using a sulforhodamine B assay after exposure for 48 h to 0.5 μmol/L of NSC134754. *C,* the growth of O19 cells with ND2 mutant was inhibited after treatment with NSC134754. Cell growth was estimated by staining with sulforhodamine *B* after exposure for 48 h to 0.5 μmol/L of NSC134754. Columns, mean from three independent experiments; bars, SD. Student's *t* test showed significance between mutant and wild type ($P < 0.01$) in the absence of NSC134754, whereas there was no significance in the presence of NSC134754. Vec, vector alone; wt, wild type; mt1, mutant.

Of note, in our study (data not shown), we also sequenced the mitochondrial genome in four other HNSCC cell lines (JHU-O11, JHU-O12, UM-22A, UM-22B), and no cell line has been found to show the specific *ND2* mutation we analyzed. The other cell line we have tested displays a variety of mitochondrial mutations in multiple respiratory complex enzymes, including ND2, with HIF1α expression. Due to the complex nature of multiple respiratory enzyme mutations in this cell line and the confounding effect this may have on assessment of an introduced, overexpressed ND2 mutation, it is difficult to determine how this would be interpreted as specifically supporting our mechanism.

***Mitochondrial ND2 mutant decreases PDH, increases phosphorylated PDH, and, thereby, increases pyruvate production, resulting in increased HIF1α accumulation.*** Recently, the cancer-specific aerobic glycolytic metabolism reported by Warburg has been linked to impairment of HIF1α degradation induced by 2-oxoglutarate analogues, such as pyruvate (12). We reasoned that the mitochondrial ND2 mutations may result in impaired respiration, resulting in the accumulation of reduced $NAD^+$ dehydrogenase and pyruvate and HIF1α stabilization. Here, the pyruvate production was determined in OKF6 cells and O19 cells after transfection with *ND2* mutant. We found significantly increased pyruvate production in *ND2* mutant-transfected OKF6 cells (5.0 ± 0.4 versus 2.8 ± 0.2 μmol/mg protein, $P < 0.01$) and O19 cells (1.6 ± 0.1 versus 1.1 ± 0.1 μmol/mg protein, $P < 0.01$) compared with corresponding wild types (Fig. 2A and B). To investigate whether increased pyruvate production could stimulate HIF1α accumulation, we gave exogenous pyruvate to OKF6 cells. HIF1α accumulation was induced by 2.9 ± 0.6-fold and 5.0 ± 1.1-fold after 4 h of treatment with 0.25 or 0.5 mmol/L pyruvate in glucose-free Krebs buffer (Fig. 2C; $P < 0.05$). Previous studies have evidenced that PDH catalyses the irreversible oxidative decarboxylation of pyruvate to acetyl-CoA, thereby linking glycolysis to the tricarboxylic acid cycle (13). It is generally believed that the pyruvate dehydrogenase reaction is the rate-limiting step in the aerobic stage of oxidation of carbohydrate fuels. To ask whether dysregulation of PDH contributed to the increased production of pyruvate, we evaluated the expression of PDH via Western blot. Compared with wild-type ND2, ND2 mutant resulted in 1.3 ± 0.2-fold, 1.4 ± 0.2-fold, and 1.3 ± 0.1-fold down-regulation of PDH in HeLa cells, OKF6 cells, and O19 cells, respectively (Fig. 2D; $n = 3$, $P < 0.05$). Because PDH has

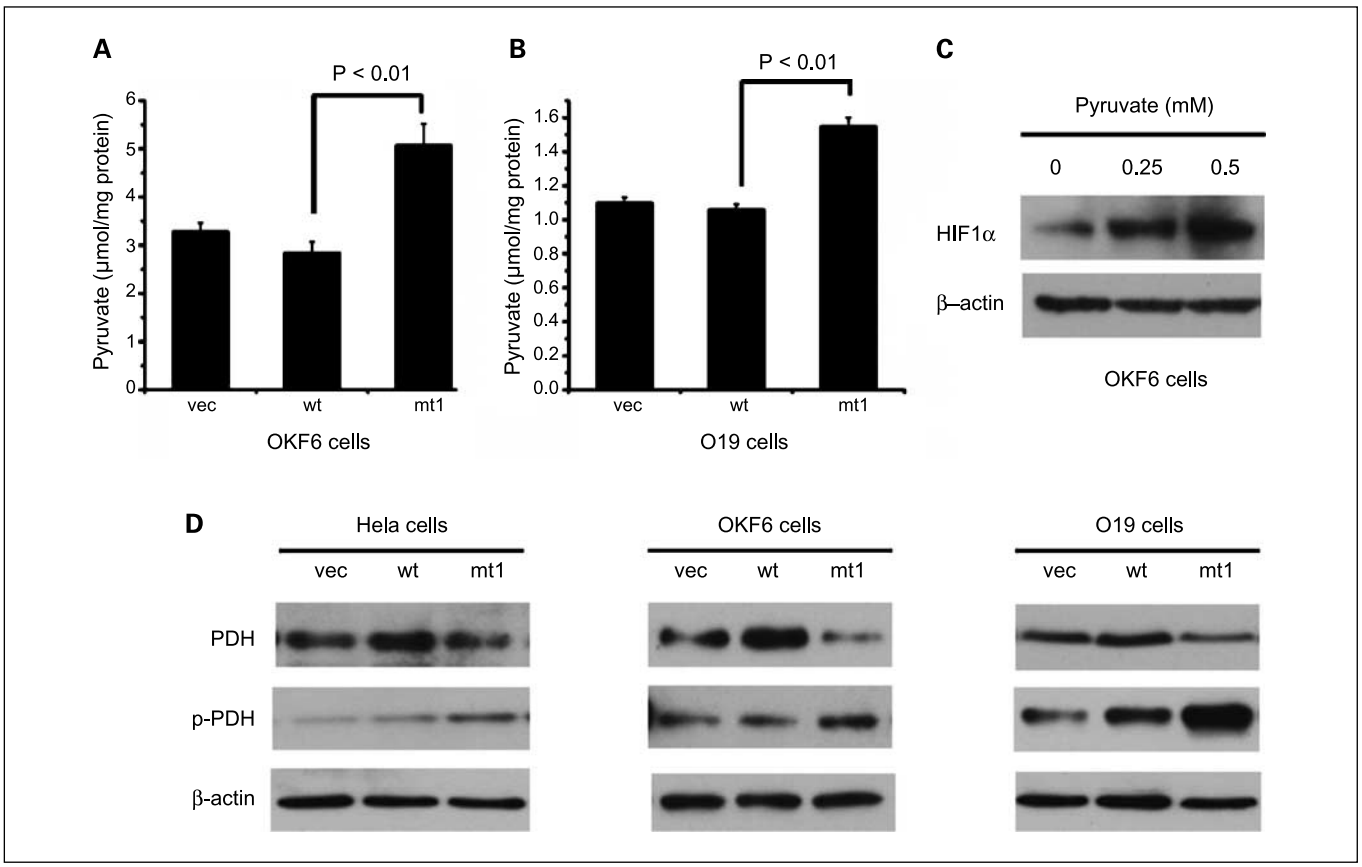


**Fig. 2.** Mitochondrial ND2 mutant decreased PDH, increased phosphorylated PDH, and thereby increased pyruvate production, resulting in increased HIF1α accumulation. *A* and *B,* the production of pyruvate in the culture buffer was measured in OKF6 cells and O19 cells. Twenty-four hours after transiently transfecting with *ND2* mutant and wild-type construct, the cells were allowed to grow in pyruvate-free media for 24 h, and then media were collected and assayed for concentration of pyruvate. Columns, mean of three individual experiments; bars, SD. Student's *t* test showed significance between mutants and wild type ($P < 0.01$). *C,* OKF6 cells were cultured for 4 h in glucose-free Krebs buffer containing 0.25 or 0.5 mmol/L pyruvate. HIF1α levels were determined after 4 h of culture. Treatment with 0.25 and 0.5 mmol/L pyruvate caused HIF1α accumulation by 2.9 ± 0.6-fold and 5.0 ± 1.1-fold, respectively, as revealed by densitometry and ImageJ software analysis. *D,* Western blot for PDH and phosphorylated PDH. Mutant 1 (*mt1*) transfection of HeLa, OKF6, and O19 cells induced decrease of PDH and increase of phosphorylated PDH compared with wild type (*wt*). After 48 h of transfection, cells were incubated with glucose-free Krebs buffer for 4 h. The cells then were harvested for Western blotting, as described in Materials and Methods. Results are representative of three independent experiments.

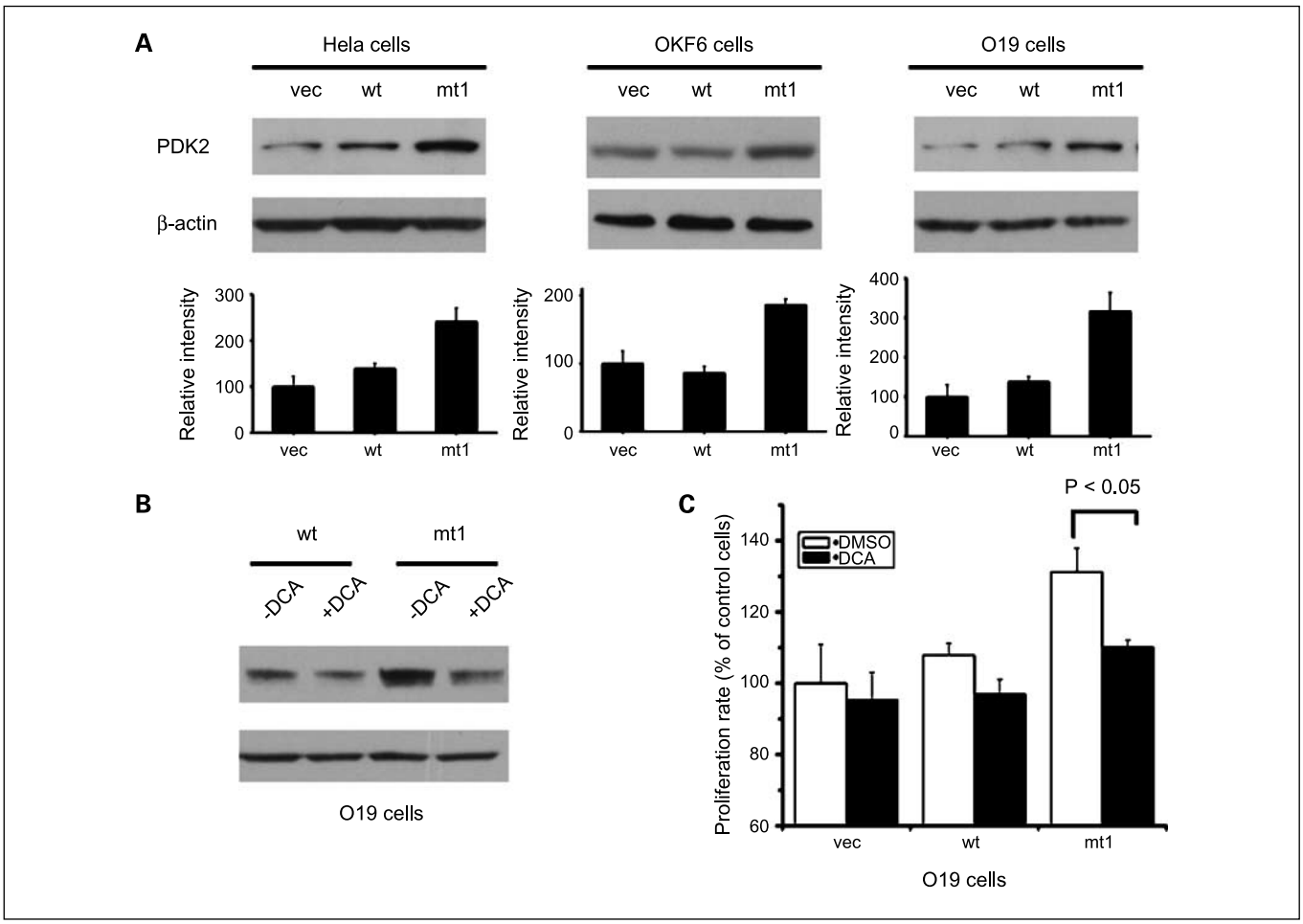


**Fig. 3.** Mitochondrial ND2 mutant elevated PDK2 expression contributing to HIF1α accumulation. *A,* the protein levels of PDK2 were determined 4 h after switching from culture medium to Krebs-Henseleit buffer in O19, HeLa, and OKF6 cells. Columns, mean of three replicate experiments; bars, SD. *B,* HIF1α levels in O19 cells stably transfected with *ND2* mutant and wild-type constructs and exposed to 2 mmol/L dichloroacetate (*DCA*) for 24 h. *C,* the growth of O19 cells, which were stably transfected with ND2 mutant, was significantly ($P < 0.05$) inhibited after treatment with 4 mmol/L dichloroacetate for 72 h. Columns, mean of three individual experiments; bars, SD.

three phosphorylation sites, including $Ser^{264}$ (the most rapidly modified site), and can be inactivated by phosphorylation (13), we further tested whether ND2 mutation resulted in conversion of PDH to phosphorylated PDH, which in turn elevated pyruvate production. To this end, anti–phosphorylated PDH ($Ser^{264}$) antibody was used to detect the expression levels of phosphorylated PDH in OKF6, HeLa, and O19 cells after transient transfection with ND2 mutant. In comparison with the wild type, phosphorylated PDH was found 1.3 ± 0.1-fold, 1.7 ± 0.2-fold, and 1.9 ± 0.2-fold higher overexpression in the cells with ND2 mutants (Fig. 2D; $n = 3$, $P < 0.05$).

***Mitochondrial ND2 mutant elevated PDK2 expression contributing to HIF1α accumulation.*** PDK2, a PDH kinase, is the key enzyme responsible for the phosphorylation of PDH at site $Ser^{264}$ (14). Thus, we examined whether our mitochondrial ND2 mutant increased the expression of phosphorylated PDH through up-regulation of PDK2. As shown in Fig. 3A, elevated expression of PDK2 (1.8 ± 0.4-fold in HeLa cells, $n = 3$, $P < 0.05$; 2.2 ± 0.2-fold in OKF6 cells, $n = 3$, $P < 0.01$; 2.3 ± 0.4-fold in O19 cells, $n = 3$, $P < 0.05$) was observed in all three cell lines transfected with the mitochondrial *ND2* mutant compared with the wild type. This suggests that mitochondrial mutants may up-regulate PDK2 expression, followed by attenuation of PDH activity and resulting in elevated pyruvate concentration, which in turn contributes to HIF1α stabilization. To determine whether PDK2 is essential for mitochondrial ND2 mutation-mediated HIF1α stabilization, we tested the effects of dichloroacetate, a PDK2 small molecule inhibitor (15). We found that, after treatment of O19 cells and OKF6 cells transfected with *ND2* mutant with 2 mmol/L dichloroacetate, the HIF1α expression level was significantly decreased (Fig. 3B and Supplementary Fig. S2A). Consistent with this result was our observation that the cell growth was inhibited in O19 cells transfected with *ND2* mutant after 3 days of treatment with 4 mmol/L dichloroacetate to a greater extent than was noted in wild type (Fig. 3C). Likewise, we also observed the growth inhibition in OKF6 cells transfected with *ND2* mutant after 2 days of treatment with 8 mmol/L dichloroacetate (Supplementary Fig. S2B).

***Mitochondrial ND2 mutant up-regulated PDK2 expression via increased ROS generation.*** We hypothesized that mitochondrial mutants may up-regulate PDK2 through increased ROS generation. To test this possibility, we determined the ROS generation in OKF6 cells transiently transfected with

mitochondrial mutant. As shown in Fig. 4A, mitochondrial ND2 mutant resulted in ~20% higher ROS yield than that in the wild type ($P < 0.01$). To investigate the effect induced by the elevated ROS yield, $H_2O_2$ titration was done to mimic the activity of mitochondrial ND2 mutation. We found that a dosage of 20 to 50 μmol/L of $H_2O_2$, after a bolus administration, could reproduce similar ROS increase in OKF6 cells (Fig. 4B). We then evaluated the PDK2 expression level in OKF6 cells, O19 cells, and HeLa cells treated with hydrogen peroxide at the concentrations of 0, 10, 20, 50, and 100 μmol/L. Our results showed that, after exposure to 20 and 50 μmol/L $H_2O_2$, PDK2 was significantly increased in OKF6 cells, O19 cells, and HeLa cells; consistently, HIF1α was also found to be up-regulated after $H_2O_2$ exposure (Fig. 4C and Supplementary Fig. S3).

***Inhibition of ROS production in mitochondrial ND2 mutant attenuated PDK2 expression and HIF1α expression.*** To investigate the effect of reduction of ROS on cells expressing mitochondrial ND2 mutant, extracellular catalase treatment was used. As shown in Fig. 5A, catalase treatment resulted in PDK2 down-regulation significantly in O19 cells transfected with the mitochondrial *ND2* mutant compared with the wild-type. Because the mitochondrion is the main organelle of ROS generation, the mito-cat construct was then used for scavenging ROS produced in O19 cells transfected with mitochondrial mutant (Fig. 5B; ref. 16). Our Western blot showed that, by introduction of mito-cat, PDK2 expression was decreased by 1.8 ± 0.2-fold in ND2 mutant cells compared with the wild type ($n = 3$, $P < 0.05$). Moreover, we found that introduction of mito-cat in OKF6 cells expressing mitochondrial mutant resulted in PDK2 down-regulation, as well as decreased expression of HIF1α (Fig. 5C). Furthermore, we observed that introduction of mito-cat in O19 cells resulted in growth inhibition ($P < 0.05$) that reversed mitochondrial mutant-mediated growth stimulation (Fig. 5D). Taken together, these suggest that mitochondrial-generated ROS plays a significant role in mitochondrial ND2 mutant-mediated head and neck cancer growth.

## Discussion

Mitochondrial mutations have been identified extensively in human HNSCC cancers, yet the functional role of mitochondrial mutation in HNSCC cancer carcinogenesis remains unclear. HIF1α is overexpressed in most of the common human cancer types, including HNSCC (17). Multiple studies of HIF1α and head and neck cancer have shown a significant association between HIF1α overexpression and poor prognosis coupled to increased patient mortality, as well as resistance to treatment

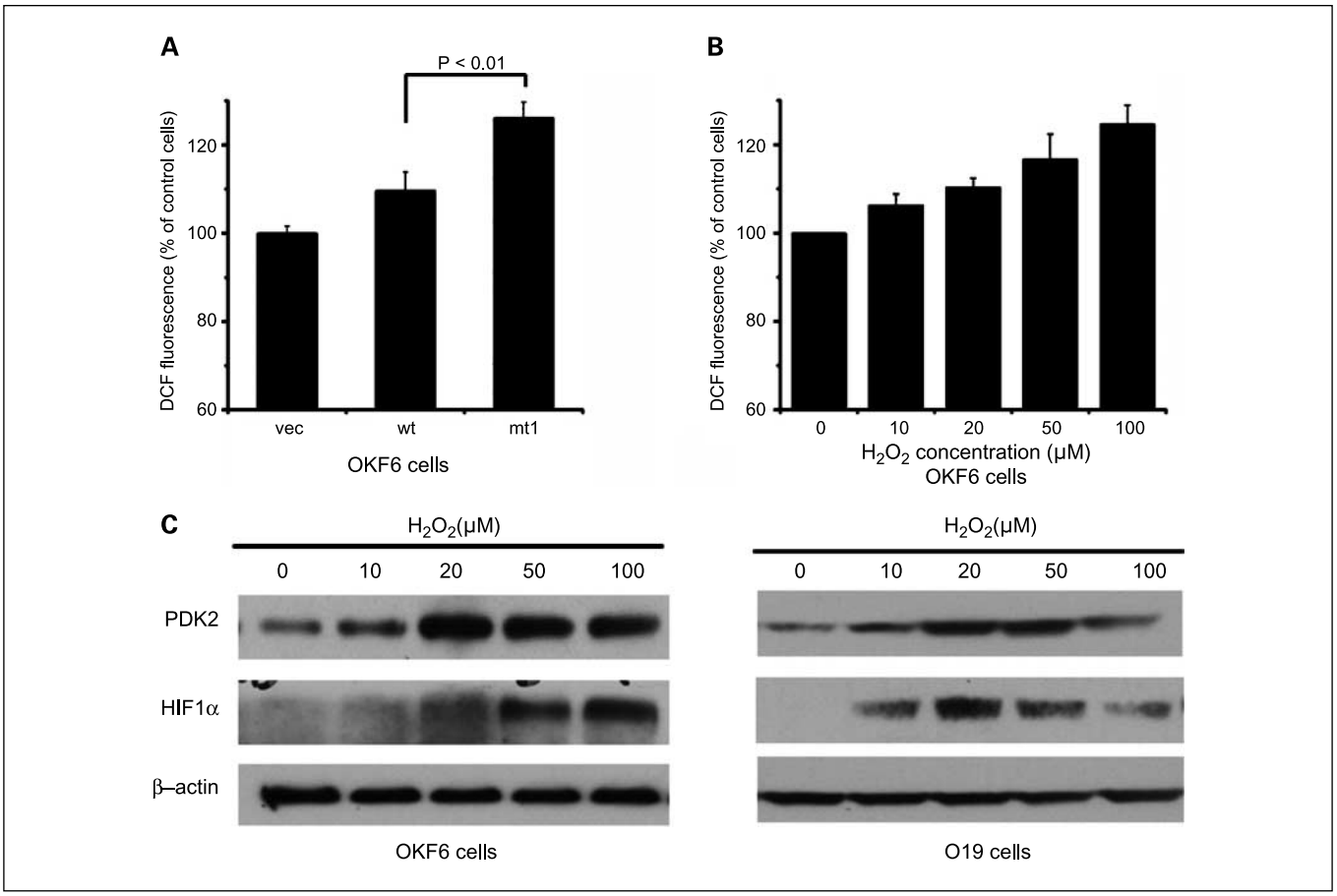


**Fig. 4.** Mitochondrial ND2 mutant up-regulated PDK2 expression via increased ROS generation. *A,* ROS generation in *ND2*-transfected OKF6 cells measured by fluorescent spectrometer. At 48 h of posttransfection, cells were harvested, and ROS was measured with a fluorescence probe DCFH-DA. Columns, mean three individual experiments; bars, SD. Student's *t* test showed significance between mutant and wild type ($P < 0.01$). *B,* ROS production in OKF6 cells exposed to repeated boluses of $H_2O_2$ (0, 10, 20, 50, and 100 μmol/L) every 20 min for 2 h. *C,* PDK2 and HIF1α levels in OKF6 cells (*left*) and O19 cells (*right*) after a bolus administration of $H_2O_2$ (0, 10, 20, 50, and 100 μmol/L) for 2 h. Blots were probed for HIF1α, PDK2, and β-actin as a loading control.

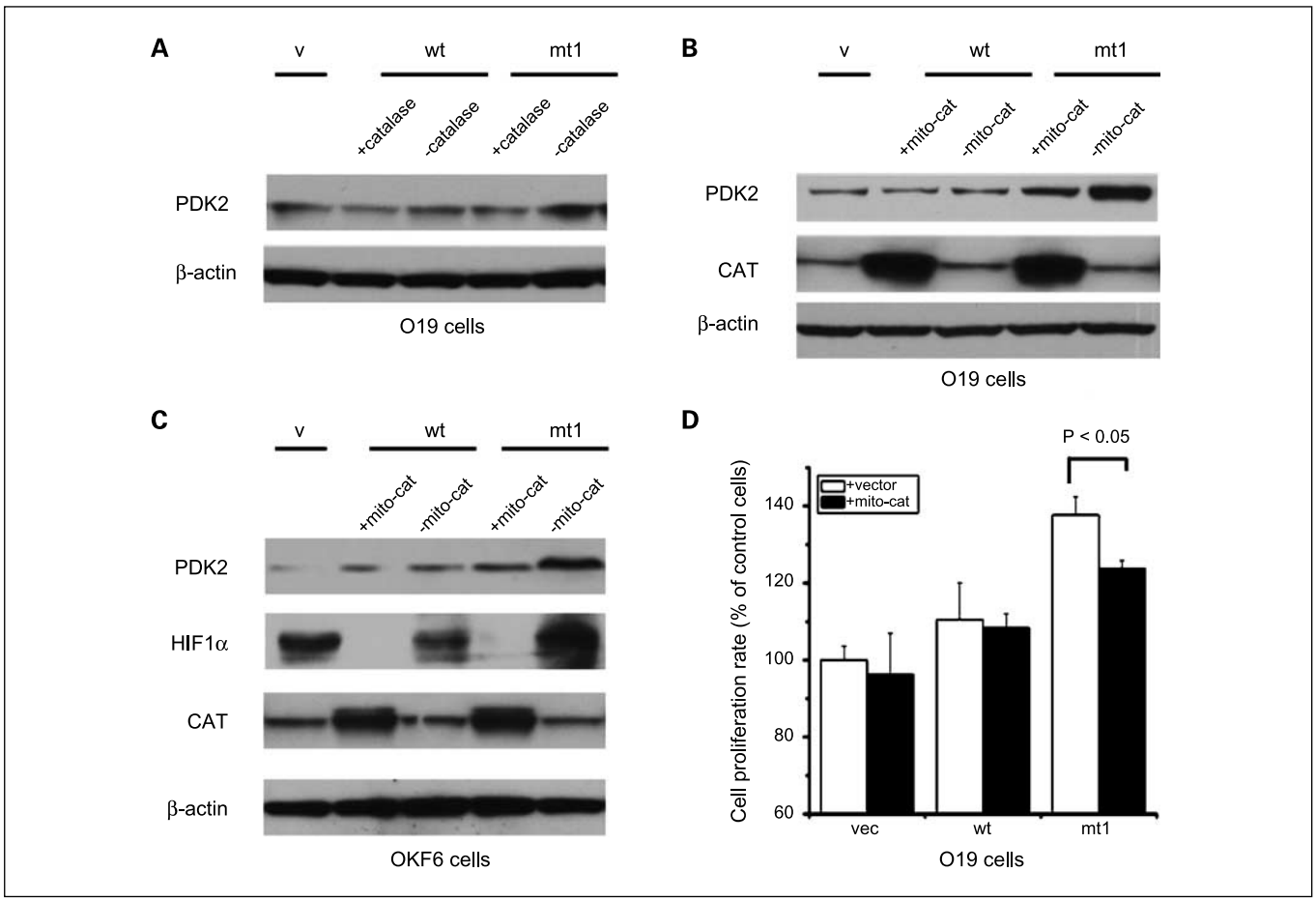


**Fig. 5.** Inhibition of ROS production in mitochondrial ND2 mutant attenuated PDK2 expression and HIF1α expression. *A,* PDK2 levels in O19 cells were transiently transfected with *ND2* mutant and wild-type construct for 24 h and then subjected to treatment with 500 units/mL catalase for 16 h. The cells were harvested for Western blot analysis, as described in Materials and Methods. +, treated with 500 units/mL catalase for 16 h; -, without catalase treatment. *B,* PDK2 and HIF1α levels in O19 cells, stably transfected with *ND2* mutant and wild-type construct, were determined after transiently transfecting of plasmid encoding mito-cat for 48 h. +, transfected with mitochondria-targeted plasmid; -, transfected with control vector alone. *C,* PDK2 and HIF1α levels in OKF6 cells stably transfected with *ND2* mutant and wild-type construct after transient transfection of plasmid encoding mito-cat for 48 h. +, transfected with mitochondria-targeted plasmid; -, transfected with vector alone. *D,* the growth of O19 cells with ND2 mutant was significantly inhibited by transient transfection of plasmid encoding mito-cat for 48 h ($P < 0.05$). Data are representative of results from three independent experiments.

(18, 19). HIF1α participates in transcriptional activation of genes that are involved in crucial aspects of cancer biology, including angiogenesis, cell survival, glucose metabolism, and invasion. In this study, we investigate the effect of mitochondrial mutation on HIF1α activation. Our data showed that HIF1α expression is enhanced in cells transfected with mutant mitochondrial *ND2*. Meanwhile, the ND2 mutant exhibited increased proliferation as comparison with the wild type, although the wild-type ND2 increased relatively the cell growth compared with the vector alone, in which the reason is unknown. Use of an HIF1α small molecule blocked mitochondrial ND2 mutant-mediated cancer cell growth (Fig. 1). These suggest that mitochondrial ND2 mutation may induce head and neck cancer development through constitutive activation of HIF1α.

Lu and colleagues recently reported that one product generated by Warburg effect, pyruvate, could dramatically increased HIF1α accumulation in cancer cells by inhibiting the prolyl hydroxylase enzyme activity, which could result in degradation of HIF1α protein through hydroxylation (12). Here, we proposed that mitochondrial ND2 mutations via production of ROS regulate enzymes, including PDH and PDH kinase, which resulted in elevated pyruvate production contributing to HIF1α accumulation. First, either O19 head and neck cancer cells or OKF6 immortal cells, which were transfected with mitochondrial *ND2* mutant, generated more pyruvate compared with the wild type. Second, extracellular treatment of pyruvate led to up-regulation of HIF1α. Third, PDH, which mediates the entry of pyruvate into tricarboxylic acid cycle, was down-regulated in cells with mitochondrial ND2 mutant. Moreover, we found that phosphorylated PDH (inactive form of PDH) and PDK2 (PDH kinase; inactivate PDH through phosphorylation) were both up-regulated in cells expressing the mitochondrial mutant.

Mitochondrial *ND2* encodes the $NAD^+$ dehydrogenase subunit 2 protein, a hydrophobic subunit of respiratory chain complex I, proposed to reside near the junction between the membrane and the peripheral arm (that projects into the mitochondrial matrix) of complex I (20). It is known that the mitochondrial respiratory chain is exquisitely tuned to

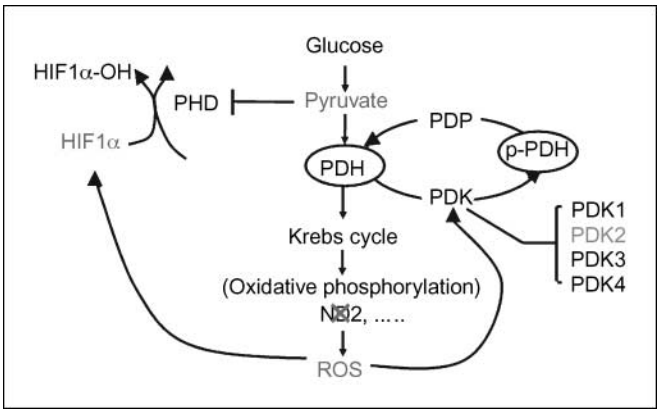


**Fig. 6.** The mechanisms of mitochondrial ND2 mutation-mediated HIF1α stabilization.

transfer electrons from $NAD^+$ dehydrogenase or FADH to a series of electron acceptors, until the final transfer to oxygen leads to the production of water. It is also known that these biochemical reactions can result in electron leakage and lead to production of ROS (21–23). The ND2 subunit is suggested to be involved in proton pumping across the inner mitochondrial membrane because of its sequence homology with a class of $Na^+/H^+$ antiporters (20). Recently, Gusdon and colleagues showed that mouse orthologue of the protective allele (mt-ND2) played a critical role in the control of mitochondrial ROS production (24). In our study, we found that more ROS was generated in cells transfected with mitochondrial *ND2* mutant compared with wild type. Extracellular treatment of cells with $H_2O_2$, a ROS mimic, led to increased HIF1α accumulation. Furthermore, we found that the expression of mito-cat could inhibit HIF1α accumulation and impede cell growth, although a partial reversal of growth stimulation with excellular mito-cat treatment was observed, likely due to the incomplete transfection efficiency during transient transfection experiments. These data suggested that mitochondrial mutation induces HIF1α accumulation through increased ROS production, consistent with results reported by Brunelle and colleagues that the expression of catalase prevented the hypoxic stabilization of HIF1α (25). In this study, enhanced ROS-induced respiratory malfunction, resulting in blockage of the tricarboxylic acid cycle, ultimately led to pyruvate accumulation and HIF1α stabilization.

To ask whether there are other pathways mediated by ROS inducing increased pyruvate production and HIF1α accumulation, we also investigated the effect of ROS on PDK2 expression. We found that extracellular treatment of $H_2O_2$ led to increased PDK2 expression. Meanwhile, application of dichloroacetate, a PDK2 small molecule inhibitor, which was previously reported to induce apoptosis and decrease proliferation (26) to cells transfected with mitochondrial *ND2* mutant, resulted in decreased HIF1α accumulation and inhibition of cell growth. These suggested that increased ROS production may contribute to HIF1α stabilization through up-regulation of PDK2. It is likely that the up-regulation of PDK2 attenuated PDH activity and triggered increased pyruvate production, which in turn lead to HIF1α stabilization. As a minor point, we also observed that with the PDK2 inhibitor dichloroacetate, there was still relatively increased proliferation in O19 mutant transfectant cells compared with the O19 wild-type transfectants (Fig. 3C). This may suggest that that there existed other pathways participating mitochondrial mutation-mediated cell proliferation.

In summary, our study suggested the mechanism of the mitochondrial mutation-mediated HNSCC carcinogenesis through HIF1α stabilization: (*a*) enhanced ROS leads to pyruvate accumulation through blocking tricarboxylic acid cycle, hence resulting in HIF1α stabilization; (*b*) increased ROS production up-regulates PDKs, followed by attenuating PDH activity and triggering high pyruvate concentration, which in turn contribute to HIF1α stabilization (Fig. 6). However, we do not rule out the increase in ROS, which stimulates constitutive activation of HIF1α through other pathways. Further study on this may help us better understand the functional role of mitochondrial mutation in the development of an invasive phenotype.

## Disclosure of Potential Conflicts of Interest

No potential conflicts of interest were disclosed.

## Acknowledgments

We thank Dr. Sigurd Lenzen for generously supplying the mitochondria-targeted catalase construct and Dr. Marianna Zahurak for kind assistance with statistical analysis.

## References

1. Wallace DC. Mitochondrial diseases in man and mouse. Science 1999;283:1482–8.
2. Jiang WW, Califano J. Mitochondrial mutations and nasopharyngeal carcinoma. Cancer Biol Ther 2004;3:1275–6.
3. Chatterjee A, Mambo E, Sidransky D. Mitochondrial DNA mutations in human cancer. Oncogene 2006;25:4663–74.
4. Zhou S, Kachhap S, Sun W, et al. Frequency and phenotypic implications of mitochondrial DNA mutations in human squamous cell cancers of the head and neck. Proc Natl Acad Sci U S A 2007;104:7540–5.
5. Mithani SK, Taube JM, Zhou S, et al. Mitochondrial mutations are a late event in the progression of head and neck squamous cell cancer. Clin Cancer Res 2007;13:4331–5.
6. Warburg O. On respiratory impairment in cancer cells. Science 1956;124:269–70.
7. Pan JG, Mak TW. Metabolic targeting as an anticancer strategy: dawn of a new era? Sci STKE 2007;2007:pe14.
8. Lu H, Forbes RA, Verma A. Hypoxia-inducible factor 1 activation by aerobic glycolysis implicates the Warburg effect in carcinogenesis. J Biol Chem 2002;277:23111–5.
9. Chandel NS, McClintock DS, Feliciano CE, et al. Reactive oxygen species generated at mitochondrial complex III stabilize hypoxia-inducible factor-1α during hypoxia: a mechanism of $O_2$ sensing. J Biol Chem 2000;275:25130–8.
10. Whitehurst AW, Bodemann BO, Cardenas J, et al. Synthetic lethal screen identification of chemosensitizer loci in cancer cells. Nature 2007;446:815–9.
11. Chau NM, Rogers P, Aherne W, et al. Identification of novel small molecule inhibitors of hypoxia-inducible factor-1 that differentially block hypoxia-inducible factor-1 activity and hypoxia-inducible factor-1α induction in response to hypoxic stress and growth factors. Cancer Res 2005;65:4918–28.
12. Lu H, Dalgard CL, Mohyeldin A, McFate T, Tait AS, Verma A. Reversible inactivation of HIF-1 prolyl hydroxylases allows cell metabolism to control basal HIF-1. J Biol Chem 2005;280:41928–39.
13. Patel MS, Korotchkina LG. Regulation of the pyruvate dehydrogenase complex. Biochem Soc Trans 2006;34:217–22.
14. Korotchkina LG, Patel MS. Site specificity of four pyruvate dehydrogenase kinase isoenzymes toward the three phosphorylation sites of human pyruvate dehydrogenase. J Biol Chem 2001;276:37223–9.
15. Baker JC, Yan X, Peng T, Kasten S, Roche TE. Marked

differences between two isoforms of human pyruvate dehydrogenase kinase. J Biol Chem 2000;275:15773–81.

**16.** Guzy RD, Hoyos B, Robin E, et al. Mitochondrial complex III is required for hypoxia-induced ROS production and cellular oxygen sensing. Cell Metab 2005;1:401–8.

**17.** Zhong H, De Marzo AM, Laughner E, et al. Overexpression of hypoxia-inducible factor 1α in common human cancers and their metastases. Cancer Res 1999;59:5830–5.

**18.** Hui EP, Chan AT, Pezzella F, et al. Coexpression of hypoxia-inducible factors 1α and 2α, carbonic anhydrase IX, vascular endothelial growth factor in nasopharyngeal carcinoma and relationship to survival. Clin Cancer Res 2002;8:2595–604.

**19.** Aebersold DM, Burri P, Beer KT, et al. Expression of hypoxia-inducible factor-1α: a novel predictive and prognostic parameter in the radiotherapy of oropharyngeal cancer. Cancer Res 2001;61:2911–6.

**20.** Brandt U. Energy converting NADH:quinone oxidoreductase (complex I). Annu Rev Biochem 2006;75:69–92.

**21.** Flemming D, Stolpe S, Schneider D, Hellwig P, Friedrich T. A possible role for iron-sulfur cluster $N_2$ in proton translocation by the NADH: ubiquinone oxidoreductase (complex I). J Mol Microbiol Biotechnol 2005;10:208–22.

**22.** Mathiesen C, Hagerhall C. Transmembrane topology of the NuoL, M and N subunits of NADH:quinone oxidoreductase and their homologues among membrane-bound hydrogenases and bona fide antiporters. Biochim Biophys Acta 2002;1556:121–32.

**23.** Friedrich T. Complex I: a chimaera of a redox and conformation-driven proton pump? J Bioenerg Biomembr 2001;33:169–77.

**24.** Gusdon AM, Votyakova TV, Reynolds IJ, Mathews CE. Nuclear and mitochondrial interaction involving mt-Nd2 leads to increased mitochondrial reactive oxygen species production. J Biol Chem 2007;282:5171–9.

**25.** Brunelle JK, Bell EL, Quesada NM, et al. Oxygen sensing requires mitochondrial ROS but not oxidative phosphorylation. Cell Metab 2005;1:409–14.

**26.** Bonnet S, Archer SL, Allalunis-Turner J, et al. A mitochondria-K+ channel axis is suppressed in cancer and its normalization promotes apoptosis and inhibits cancer growth. Cancer Cell 2007;11:37–51.

Clinical Cancer Research

# Mitochondrial Mutations Contribute to HIF1α Accumulation via Increased Reactive Oxygen Species and Up-regulated Pyruvate Dehydrogenease Kinase 2 in Head and Neck Squamous Cell Carcinoma

Wenyue Sun, Shaoyu Zhou, Steven S. Chang, et al.

*Clin Cancer Res* 2009;15:476-484.